DWBA-G calculations of electron impact ionization of noble gas atoms

A S Kheifets†

Research School of Physical Sciences and Engineering, The Australian National University, Canberra ACT 0200, Australia

A Naja, E M Staicu Casagrande and A Lahmam-Bennani

Université Paris-Sud 11, Laboratoire des Collisions Atomiques et Moléculaires (LCAM), Bât. 351, 91405 Orsay Cedex, France

CNRS-LCAM (UMR 8625), Bât. 351, 91405 Orsay Cedex, France

Abstract. We perform calculations of electron impact ionization of noble gas atoms within the distorted wave Born approximation (DWBA) corrected by the Gamow factor (G) to account for the post-collision interaction. We make an extensive comparison with experimental data on He $1s^2$, Ne $2s^2$, $2p^6$ and Ar $3p^6$ under kinematics characterized by large energy transfer and close to minimum momentum transfer from the projectile to the target. For all atoms, good agreement between theory and experiment is achieved. In the case of Ar, the disagreement of experimental data with theory reported earlier by Catoire *et al* [J. Phys. B **39**, 2827 (2006)] is reconciled.

PACS numbers: 34.80.Dp, 34.50.Fa, 34.80.-i

† Corresponding author: A.Kheifets@anu.edu.au

1. Introduction

Single ionization of atoms by electron impact is a well researched topic (see, e.g. a recent book by McCarthy & Weigold (2005) and a review by Schulz & Madison (2006) and references therein). Physical mechanisms driving electron impact ionization of an atomic shell are well understood. For an energetic projectile with the incident energy significantly larger than the ionization potential, the single knock-out collision ejects the initially bound target electron into continuum. Multiple collisions of the projectile with the target can be safely neglected in this case. This justifies a theoretical description within the lowest order perturbation theory known as the first Born approximation (FBA). In the meantime, the distorting effect of the target potential on the continuum electron states, especially the slow ejected electron moving in the field of an ion, are generally strong and should be treated non-perturbatively. Account for these physical processes constitute the so-called distorted wave Born approximation (DWBA). Since the pioneering work by Madison *et al* (1977), numerous realizations of DWBA have been reported in the literature (Whelan *et al* 1993, Kheifets 1993, McCarthy 1995, Mazevet *et al* 1998), to name just a few. Relativistic extension of DWBA is also available (Nakel & Whelan 1999). There was also developed a hybrid of DWBA and the R-matrix model (DWB-RM) which took into account the same interactions of the projectile with the target but was more elaborate in description of many-electron processes in the ionized target (Bartschat & Burke 1987).

When the scattered and ejected electron acquire comparable energies, their post-collision interaction (PCI) is also strong and should be treated to all orders. This can be achieved within the so-called BBK method (Brauner *et al* 1991). The basic idea is that the final state is described by a product of three Coulomb waves, (hence the alternative name of 3C). The main characteristic of the model is that both the PCI between the three Coulomb particles in the final state and multiple scattering effects are included. The drawback of the BBK method is that the distorting effects of the target on the projectile are ignored. This limits application of the BBK method to light targets such as the H and He atoms. For these atoms, however, more elaborate non-

perturbative methods, for example but not exclusively, the convergent close-coupling (CCC) (Bray *et al* 2002) and the exterior exterior complex scaling (ECS) (Rescigno *et al* 1999) produce, generally, more accurate results. A merger of the DWBA and BBK methods resulted in development of the so-called 3DWBA method (Jones & Madison 1994) which could take into account both the key interactions of the DWBA model and the PCI. This has been successfully demonstrated in the case of (e,2e) on the $4s^2$ shell of Kr (Haynes *et al* 2003).

Owing to massive experimental and theoretical efforts, the field of electron impact single ionization of atoms by energetic projectiles was considered to be fairly well explored. Good agreement between theory and experiment was achieved in the most demanding coincidence (e,2e) mode for a wide range of targets other than H or He. Noble gas atoms from Ne to Xe were particularly well studied (Lahmam-Bennani 2002). Latest experimental data on Mg were also found in good agreement with DWBA calculations (Bolognesi *et al* 2008).

That is why a recent measurement of (e,2e) on Ar by Catoire *et al* (2006) came as a surprise as it was in manifest disagreement with both the DWB-RM and BBK calculations. A relatively high energy of the projectile $E_0 = 721$ eV as well as the energies of both outgoing electrons $E_1 = 500$ eV and $E_2 = 205$ eV clearly warranted a successful application of the DWBA or DWB-RM methods. Theoretical results, however, were quite disappointing. The binary peak was significantly overestimated by the DWB-RM calculation whereas the BBK model predicted the right magnitude of the binary peak but showed virtually no recoil peak. Going beyond the FBA by considering repeated interactions of the projectile with the target (the so-called DWB-RM2 model) did not change theoretical results in an appreciable way.

In the follow-up paper by Naja *et al* (2008), the authors concluded that argon was a somewhat complicated target and turned their attention to a lighter noble gas atom - neon. For this target, they were able to achieve a good agreement between two independent sets of experiments and the DWBA and DWB-RM calculations. Particularly good agreement was reported for the DWBA calculation corrected for the

PCI effects by the so-called Gamow factor. This factor, also known as the Coulomb density of states (Brauner *et al* 1991) or N_{ee} factor (Rouvellou *et al* 1998), represents the normalization constant of the two-body Coulomb function describing the interaction of the two continuum electrons in the final state.

In the present manuscript we demonstrate that the DWBA-G model (DWBA corrected by the Gamow factor) describes very well the experimental data on Ar reported previously by Catoire *et al* (2006). We also validate this model by making an extensive comparison with experimental data on He $1s^2$, Ne $2s^2$, $2p^6$ and Ar $3p^6$ taken at the scattered electron energy $E_1 = 500$ eV, the scattering angle $\theta_1 = 6^\circ$ and ejected electron energies $E_2 = 37$, 74 and 205 eV. Such a kinematics is characterized by large energy transfer and close to minimum momentum transfer from the projectile to the target. Except for the He $1s$ and Ar $3p$ measurements at $E_2 = 205$ eV reported previously by Catoire *et al* (2006), all the experimental data are new and performed on purpose of making an exhaustive comparison with the theory. A wide range of targets and varying ejected electron energy allows to observe some trends which reveal the underlying physics of the (e,2e) reaction on closed-shells atomic targets.

The paper is organized as follows. In Section 2 we outline the theoretical model. In Section 3 we give a brief account of experimental procedures. We compare and discuss experimental and theoretical results in Section 4. The atomic units are used throughout the paper unless otherwise indicated.

2. Theory

In this section, we follow closely derivations of Kheifets (1993). This earlier paper, however, was concerned with electron impact ionization of He and the associated formalism exploited the two-electron structure of the target. In the present work, we extend this formalism to an arbitrary closed-shell target. We consider an (e,2e) reaction in which the incident electron $\boldsymbol{k}_0$ impinges onto the atomic shell i resulting in two outgoing electrons $\boldsymbol{k}_1$ (scattered) and $\boldsymbol{k}_2$ (ejected) in the final state. According to a general formalism (see, e.g. Rouvellou *et al* (1998)), the fully resolved triply differential

cross-section (TDCS) of such a reaction can be written as

$$\frac{d^3\sigma}{d\Omega_1\, d\Omega_2\, dE_2} = \frac{1}{(2\pi)^5}\frac{k_2\ k_1}{k_0}\ \frac{N_i}{2l_i{+}1}\sum_{m_i}\ \frac{1}{4}\sum_S (2S+1)\left|T_S(\boldsymbol{k}_0,\boldsymbol{k}_2,\boldsymbol{k}_1)\right|^2 \quad , \tag{1}$$

where averaging is performed over the magnetic quantum number of the target electron m_i and the total spin S of the scattering system *projectile + atom*. The continuum states are normalized to $\langle \boldsymbol{k}|\boldsymbol{k}'\rangle = (2\pi)^3\delta(\boldsymbol{k}-\boldsymbol{k}')$ and have the asymptotics $\langle \boldsymbol{r}|\boldsymbol{k}\rangle \approx e^{i\boldsymbol{k}\cdot\boldsymbol{r}}$. The matrix element T_S is the combination of the direct D_i and exchange E_i Coulomb matrix elements:

$$\sum_S (2S+1)\left|T_S\right|^2 = \left[T_0 + 3T_1^2\right] = \left[(D_i+E_i)^2 + 3(D_i-E_i)^2\right] \ . \tag{2}$$

For a closed-shell atomic target, we can adopt the electron-hole formalism and refer to the initial atomic state as the vacuum state. The final state of the target has one hole i and one electron $\boldsymbol{k}_2$. In this formalism, the direct and exchange Coulomb matrix elements can be written as

$$D_i = \langle \boldsymbol{k}_1\boldsymbol{k}_2|V|\boldsymbol{k}_0 i\rangle \quad , \quad E_i = \langle \boldsymbol{k}_2\boldsymbol{k}_1|V|\boldsymbol{k}_0 i\rangle \quad , \quad V = |\boldsymbol{r}_1-\boldsymbol{r}_2|^{-1} \tag{3}$$

The electron-hole formalism is illustrated in Figure 1. Here we employ the following graphical symbols. A solid line with an arrow pointing to the left denotes a hole whereas an arrow pointing to the right indicates a continuum electron state. The wavy line stands for the Coulomb inter-electron interaction. The left diagram of Figure 1 illustrates the direct Coulomb matrix element D_i. The exchange matrix element E_i can be exhibited by a similar graph in which the electrons $\boldsymbol{k}_1$ and $\boldsymbol{k}_2$ are swapped.

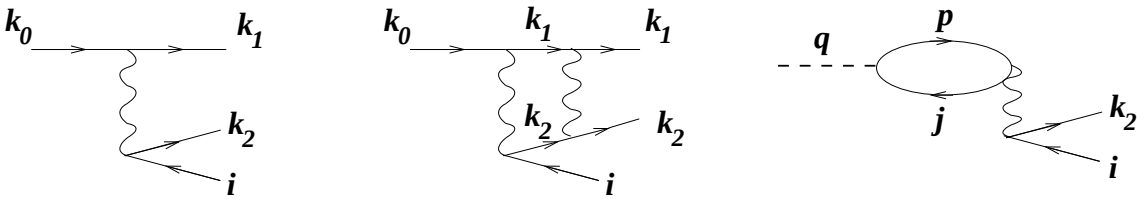

Figure 1. Left: Graphical representation of the direct matrix element D_i in Equation (3). Arrows to the left and right denote the hole and electron states, respectively. The wavy line exhibits the Coulomb interaction. Center: Post-collision interaction in the final state accounted for by the Gamow factor (9). Right: Inter-shell correlation of the RPA type represented by Equation (13). The dashed line denotes the Born operator $\exp(i\boldsymbol{q}\cdot\boldsymbol{r})$.

We separate the radial and angular parts $\langle \boldsymbol{r}|i\rangle = r^{-1}P_{n_i l_i}(r)Y_{l_i m_i}(\hat{\boldsymbol{r}})$ and employ a partial wave expansion

$$\langle \boldsymbol{r}|\boldsymbol{k}\rangle = \frac{(2\pi)^{3/2}}{k^{1/2}} \sum_{lm} e^{\pm i\delta_l} i^l Y^*_{lm}(\hat{\boldsymbol{k}}) Y_{lm}(\hat{\boldsymbol{n}}) \frac{1}{r} P_{El}(r) \tag{4}$$

with the continuum radial wave functions normalized on the energy scale and having the asymptotics $P_{El}(r \to \infty) \propto \sqrt{\frac{2}{\pi k}}\,\sin(kr - \frac{l\pi}{2} + \delta_l)$. The plus sign in the phase factor corresponds to the incident electron $\boldsymbol{k}_0$ whereas the minus sign should be taken for the two outgoing electrons $\boldsymbol{k}_1$ and $\boldsymbol{k}_2$. We align the z axis with the vector $\boldsymbol{k}_0$ and perform the angular integration of the products of three spherical harmonics according to Varshalovich *et al* (1988). Finally, we get the following expression for the direct Coulomb matrix element:

$$D_{m_i} = \frac{(2\pi)^{9/2}(4\pi)^{-1/2}}{(k_0 k_1 k_2)^{1/2}} \sum_{\substack{l_0 l_1 l_2\, \lambda \\ m_1 m_2}} e^{i(\delta_{l_0}+\delta_{l_1}+\delta_{l_2})}\; i^{l_0-l_1-l_2}\; \hat{l}_0\; Y_{l_1 m_1}(\hat{\boldsymbol{k}}_1) Y_{l_2 m_2}(\hat{\boldsymbol{k}}_2) \tag{5}$$
$$(-1)^{m_2} \begin{pmatrix} l_1 & \lambda & l_0 \\ -m_1 & m_1 & 0 \end{pmatrix} \begin{pmatrix} l_i & \lambda & l_2 \\ -m_i & m_1 & m_2 \end{pmatrix} \langle k_1\, k_2 \parallel V_\lambda \parallel k_0\, i\rangle \ .$$

Here we introduced a reduced Coulomb matrix element:

$$\langle k_1\, k_2 \parallel V_\lambda \parallel k_0\, i\rangle = \hat{l}_0\, \hat{l}_2\, \hat{l}_1\, \hat{l}_i \begin{pmatrix} l_1 & \lambda & l_0 \\ 0 & 0 & 0 \end{pmatrix} \begin{pmatrix} l_i & \lambda & l_2 \\ 0 & 0 & 0 \end{pmatrix} R^\lambda_{l_0\, l_2\, l_1\, l_i}(k_0, k_1, k_2, n_i) \tag{6}$$

defined in terms of a Slater integral

$$R^\lambda_{l_0\, l_2\, l_1\, l_i}(k_0, k_1, k_2, n_i) = \int_0^\infty dr_1 \int_0^\infty dr_2 P_{E_0}(r_1) P_{E_1}(r_2) \frac{r_<^\lambda}{r_>^{\lambda+1}} P_{E_2}(r_2) P_{n_i l_i}(r_2) \ , \tag{7}$$

where $r_<$ and $r_>$ are, respectingly, the smaller and larger of the coordinates r_1, r_2. We also introduced the hat symbol $\hat{l} = \sqrt{2l+1}$. The exchange matrix element E_{m_i} is expressed by an equation similar to (5) in which the reduced Coulomb matrix element is changed to

$$\langle k_1\, k_2 \parallel V_\lambda \parallel k_0\, i\rangle \to (2\lambda+1) \sum_{\lambda'} (-1)^{\lambda+\lambda'} \begin{Bmatrix} l_1 & \lambda & l_0 \\ l_2 & \lambda' & l_i \end{Bmatrix} \langle k_2\, k_1 \parallel V_{\lambda'} \parallel k_0\, i\rangle \tag{8}$$

In order to include the long-range Coulomb interaction in the final state, which is illustrated by the middle diagram of Figure 1, the final two-electron state should be multiplied by the Coulomb factor (Brauner *et al* 1991):

$$C(\alpha, \boldsymbol{k}, \boldsymbol{R}) = \Gamma(1 - i\alpha) e^{-\pi\alpha/2}\, {}_1F_1\Big[i\alpha, 1;\, -i(kR + \boldsymbol{k}\cdot\boldsymbol{R})\Big]$$

Here $\alpha = 1/k$, $\boldsymbol{k} = \boldsymbol{k}_1 - \boldsymbol{k}_2$ and $\boldsymbol{R} = \boldsymbol{r}_1 - \boldsymbol{r}_2$. The normalization factor is known as the Gamow factor or the Coulomb density of states:

$$\left|\Gamma(1 - i\alpha)e^{-\pi\alpha/2}\right|^2 = \frac{2\pi\alpha}{e^{2\pi\alpha} - 1} \equiv G(k) \tag{9}$$

Explicit evaluation of the matrix elements D_i and E_i modified by the Coulomb factor is cumbersome. We argue, however, that the largest effect of the PCI is contained in the Gamow factor alone. We can prove this in a special case of a very fast projectile and a relatively slow ejected electron. In this case, we can represent the incident and scattered electron by the plane waves $\langle \boldsymbol{r}|\boldsymbol{k}\rangle = e^{i\boldsymbol{k}\cdot\boldsymbol{r}}$ and neglect the exchange term which constitutes the so-called plane-wave Born approximation (PWBA). The Coulomb interaction in this case is reduced to the Born operator:

$$D_i = \langle \boldsymbol{k}_1\boldsymbol{k}_2|V|\boldsymbol{k}_0 i\rangle \approx \langle \boldsymbol{k}_2|M(\boldsymbol{q})|i\rangle \ , \tag{10}$$

where

$$M(\boldsymbol{q}) = e^{i\boldsymbol{q}\cdot\boldsymbol{r}} \int d^3R\, e^{i\boldsymbol{q}\cdot\boldsymbol{R}} \frac{1}{R} = e^{i\boldsymbol{q}\cdot\boldsymbol{r}} \lim_{\gamma\to 0} 4\pi \int_0^\infty \frac{\sin qR}{q} e^{-\gamma R}\, dR = \frac{4\pi}{q^2} e^{i\boldsymbol{q}\cdot\boldsymbol{r}} \ . \tag{11}$$

Here $\boldsymbol{R} = \boldsymbol{r}_1 - \boldsymbol{r}_2$ and $\boldsymbol{q} = \boldsymbol{k}_0 - \boldsymbol{k}_1$ is the momentum transfer from the projectile to the target. Using the integral representation of the hypergeometrical function (Landau & Lifshitz 1985), we can write the Born operator modified by the Coulomb factor in the integral form similar to Equation (11). In result, we get

$$\begin{aligned} \overline{M}(\boldsymbol{q}) \quad &= \frac{4\pi}{q^2}\, \sqrt{G(k)} \left\{ -\frac{1}{2\pi i} \int_C (-t)^{\alpha-1}(1-t)^{-\alpha}(1-tz)^{-1}\, dt \right\} \\ &= \frac{4\pi}{q^2}\, \sqrt{G(k)}\ {}_2F_1\left(i\alpha, 1, 1;\, 2\boldsymbol{q}\cdot\boldsymbol{k}/q^2\right) = \frac{4\pi}{q^2}\, \sqrt{G(k)}\, \left(1 - \frac{2\boldsymbol{q}\cdot\boldsymbol{k}}{q^2}\right)^{-i\alpha} \end{aligned} \tag{12}$$

Here we used Eq. (15.1.8) of Abramowitz & Stegun (1975). The factor in the bracket is positive and hence the modulus squared of its imaginary power is equal to one. Thus, the Gamow factor alone accounts for the bulk of the PCI effect.

Another type of many-electron correlations which can be accounted for in the present model is ionization of the inner atomic shell by creating a virtual electron-hole pair in the nearby outer shell. This type of correlation, illustrated by the right diagram of Figure 1, is known to modify significantly photoionization cross-section of the valence shells of noble gas atoms (Amusia 1990). Similar effect can be noticeable in

electron impact ionization as well. To account for such an effect, we employ the random phase approximation (RPA) and modify the Born matrix element in Equation (10) by the following integral equation:

$$\langle \boldsymbol{k}_2|\mathcal{M}(\boldsymbol{q})|i\rangle \;= \langle \boldsymbol{k}_2|M(\boldsymbol{q})|i\rangle \;+ \sum\!\!\!\!\!\!\int_{j,\boldsymbol{p}} \frac{\langle \boldsymbol{p}|\mathcal{M}(\boldsymbol{q})|j\rangle \;\langle \boldsymbol{k}_2\, j|V|\boldsymbol{p}\, i\rangle}{k_2^2 - \varepsilon_i - p^2 + \varepsilon_j + i\delta} \tag{13}$$

Now we turn our attention to calculation of the bound target orbitals $P_{n_i l_i}(r)$ and continuum orbitals P_{El} and their phases δ_l. We obtain the target orbitals using the self-consistent field Hartree-Fock (SCFHF) method implemented in the computer code by Chernysheva *et al* (1976). These orbitals are then frozen to obtain the frozen-core Hartree-Fock (FCHF) potential which is then fed into a set of FCHF equations solved by the computer code of Chernysheva *et al* (1979).

It is known that the virtual electron-hole excitations within a single atomic shell (the right diagram of Figure 1 with $i = j$) can be accounted for within the standard electron-hole PWBA formalism by a particular choice of the ejected electron continuum orbitals (Amusia 1990). These orbitals should be calculated in the FCHF potential of the singly ionized target with the hole i. A similar treatment should be given to the scattered electron but its interaction with the ionized target is less important since the projectile is fast. As to the incident electron, its continuum orbitals should be calculated in the field of the neutral target as the hole is created after the encounter of the projectile with the target.

After the radial orbitals and phases are defined, they are plugged into Eqs. (5–7). The Born matrix element is evaluated by a partial wave expansion similar to Eq. (5) :

$$\langle \boldsymbol{k}_2|M(\boldsymbol{q})|i\rangle \propto \frac{1}{q^2}\sum_{Jl} e^{i\delta_l} i^{J-l} Y_{lm_i}(\hat{\boldsymbol{k}}_2)\,(-1)^{m_i} \begin{pmatrix} l & J & l_i \\ -m_i & 0 & m_i \end{pmatrix} \hat{J}^2\, D_{Jl\,n_i l_i}(q,E) \tag{14}$$

Here the quantization axis z is directed along the vector of the momentum transfer $\boldsymbol{q}$. The reduced matrix element is defined as

$$D_{Jl\,n_i l_i}(q,E) = \hat{l}\hat{l}_i \begin{pmatrix} l & J & l_i \\ 0 & 0 & 0 \end{pmatrix} \int dr\, P_{El}\, j_J(qr)\, P_{n_i l_i} \tag{15}$$

A set of RPA equations (13) is solved by using the computer code of Chernysheva *et al* (1975).

3. Experiment

The experimental set-up currently in use in Orsay, which combines three high-efficiency, multi-angle toroidal electrostatic energy analyzers was described in detail elsewhere (Catoire *et al* 2007). The experimental procedure is essentially identical to the one reported in Naja *et al* (2007) and Catoire *et al* (2006). Briefly, a monochromatic incident electron beam collides with the gas jet formed at the collision centre. A coplanar geometry is used, where all electrons are observed in the collision plane defined by the incident and scattered momentum vectors $\boldsymbol{k}_0$ and $\boldsymbol{k}_1$, respectively. The 'slow' ejected electrons (designated with an index 2) are multi-angle analyzed in a double toroidal analyzer, with energies $E_2 = 37$, 74 and 205 eV, successively, and over the angular ranges $\theta_2 = 20^\circ - 150^\circ$ and $210^\circ - 340^\circ$, where 0° is defined by the incident beam direction. In the off-line analysis, the total θ_2 -angular range is divided into sectors of width $\Delta\theta_2 = 5^\circ$. The 'fast', forward-scattered electron (indexed 1) is collected by the third toroidal analyzer (Catoire *et al* 2007) at the scattered energy $E_1 = 500$ eV. In the present work, the $\boldsymbol{k}_1$-electron is simultaneously observed at two symmetrical angles, $\theta_1 = +(6^\circ \pm 0.25^\circ)$ and $\theta_1 = -(6^\circ \pm 0.25^\circ)$ as mechanically imposed by input slits at the entrance to the electrostatic lenses associated with the toroidal analyzer. The incident energy E_0 is consequently adjusted to fulfill the energy conservation requirement for the target under study, $E_0 = E_1 + E_2 + IP$, where IP is its ionization potential.

Because of a low coincidence rate due, in particular, to the high ejection energy used, all the three toroidal analyzers were operated at a reduced energy resolution, $\Delta E_1 \sim \pm 2.3$ eV and $\Delta E_2 \sim \pm 1$eV, resulting in a coincidence energy resolution (Dupre *et al* 1991), $\Delta E_{\rm coin} \sim \pm 2.5$ eV (the energy dispersion of the incident beam is negligible, $\Delta E_0 \sim \pm 0.25$ eV). The choice of a modest resolution was deliberate in order to be able to measure the inner $2s$ orbital of neon ($IP = 48.5$ eV). This orbital is well isolated from the other outer orbitals and from the neighbouring satellite structures, $2s^2 2p^4 3d$ (Samardzic *et al* 1993), but being an inner one its ionization cross section is appreciably smaller. Combining all these figures, the momentum transfer resolution amounts to $\Delta q = \pm 0.02$ au while the spread in the momentum transfer direction is

about $\Delta\theta_q \sim \pm 1°$.

Finally, we note that the He data discussed here are similar to those published in Catoire *et al* (2006) and Staicu Casagrande *et al* (2008), though it was preferred here to re-measure them immediately before and after the new Ne and Ar runs for more consistency, on the one hand, and for monitoring the good response of the spectrometer, on the other hand. The new He sets of data are found to be in very good agreement with the older ones and in fair agreement with CCC calculations, thus validating the experimental procedure.

4. Results and Discussion

4.1. Helium

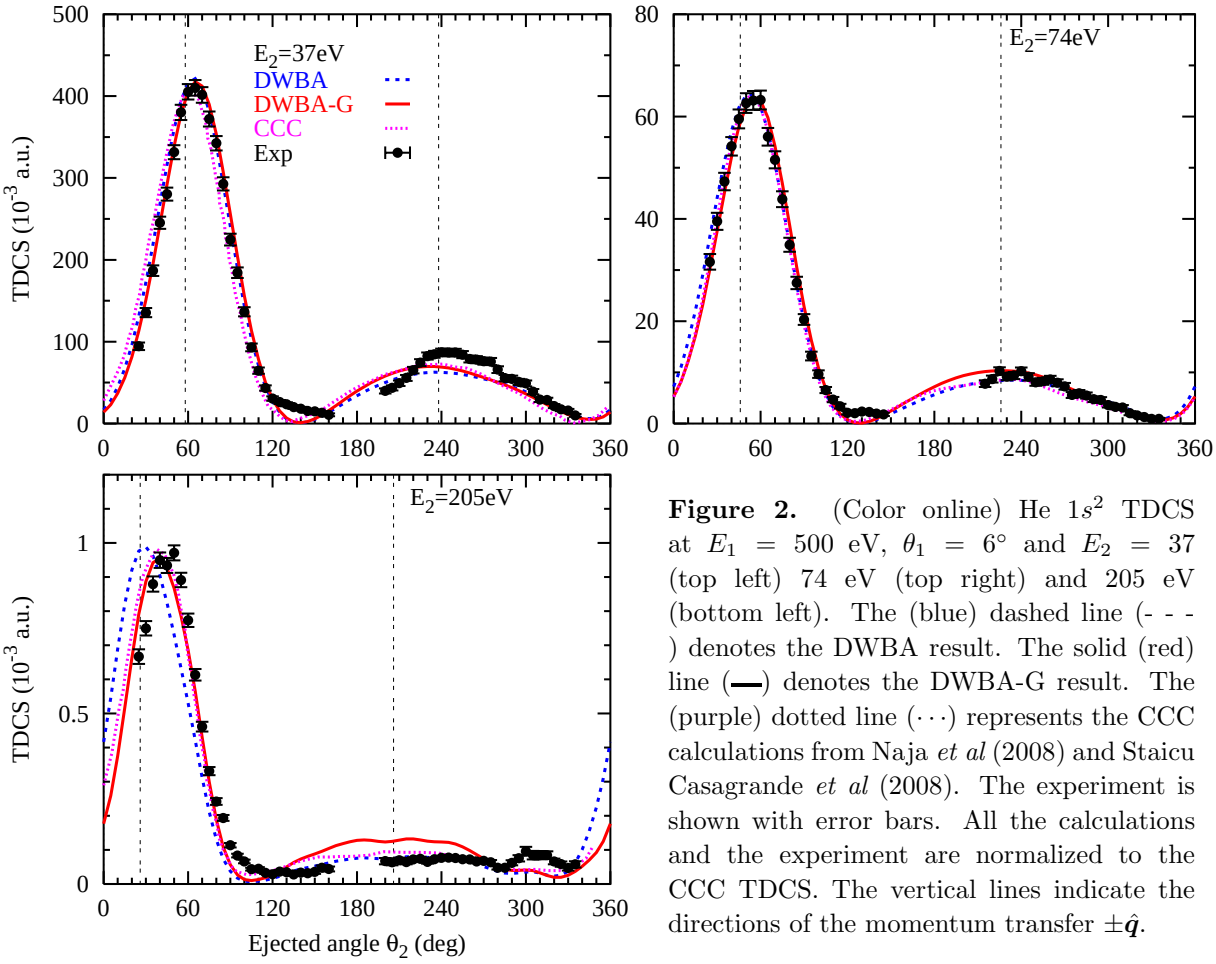

Figure 2. (Color online) He $1s^2$ TDCS at $E_1 = 500$ eV, $\theta_1 = 6°$ and $E_2 = 37$ (top left) 74 eV (top right) and 205 eV (bottom left). The (blue) dashed line (- - -) denotes the DWBA result. The solid (red) line (—) denotes the DWBA-G result. The (purple) dotted line ($\cdots$) represents the CCC calculations from Naja *et al* (2008) and Staicu Casagrande *et al* (2008). The experiment is shown with error bars. All the calculations and the experiment are normalized to the CCC TDCS. The vertical lines indicate the directions of the momentum transfer $\pm\hat{\boldsymbol{q}}$.

The TDCS of (e,2e) on the He atom is presented in Figure 2 corresponding to the

scattered electron energy and angle of $E_1 = 500$ eV and $\theta_1 = 6^\circ$. The three panels display the TDCS at the ejected electron energies of $E_2 = 37$, 74 and 205 eV. The corresponding values of the momentum transfer are $q = 0.74$, 0.87 and 1.44 a.u. The (blue) dashed line denotes the DWBA result while the (red) solid line denotes the DWBA-G result. The CCC calculations from Naja *et al* (2008) and Staicu Casagrande *et al* (2008) are shown by the (purple) dotted line. This model is known to produce very accurate TDCS results for electron impact single ionization of He when the residual ion is left in its ground state. Accordingly, we normalized both the DWBA and DWBA-G as well as the experiment to the CCC TDCS. To scale DWBA to CCC, a normalization factor close to 1 was applied. The Gamow factor is known to violate normalization strongly. So some additional rescaling to CCC was required with a normalization factor of the order of ~ 2.

As we see from the figure, the DWBA calculation is in agreement with experimental data for $E_2 = 37$ eV and 74 eV. For this ejected electron energies, the disparity between $E_1 = 500$ eV and E_2 is very large and the Gamow factor corrections are insignificant. However, for $E_2 = 205$ eV this situation changes and the DWBA-G calculation is much closer to the CCC calculation and to the experiment than DWBA displaying a significant angular shift from the direction of the momentum transfer.

It is seen from the figure that the magnitude of the TDCS is rapidly decreasing as the energy of the ejected electron increases from 37 eV to 205 eV. This is understandable since the TDCS is roughly proportional to q^{-4}. Also noticeable is a steady decrease of the recoil peak intensity relative to the magnitude of the binary peak as the energy of the ejected electron increases. The origin of the recoil peak was explained qualitatively by Vriens (1969) who attributed it to reflection of the ejected electron from the atomic potential well. The relative recoil-to-binary intensity ratio is proportional to the reflection coefficient which is decreasing as the energy of the ejected electron is getting larger. As it will be demonstrated in the next section, this is not always the case. For instance, the recoil-to-binary intensity ratio is, in fact, increasing with the ejected electron energy in the case of (e,2e) on Ne $2s^2$.

4.2. Neon

The TDCS of (e,2e) on the Ne $2s^2$ shell is presented in Figure 3 corresponding to the scattered electron energy and angle of $E_1 = 500$ eV and $\theta_1 = 6°$. The top two panels display the TDCS at the ejected electron energies of $E_2 = 37$ and 74 eV. The (blue) dashed line denotes the DWBA result while the solid (red) line denotes the DWBA-G result normalized to that of DWBA. As in the case of He, the Gamow factor correction improves agreement with experiment, especially for 74 eV ejected electron energy.

It is noticeable that, in contrast to the He $1s^2$ ionization, the relative intensity of the recoil peak is larger for 74 eV ejected energy as compared to the lower energy of 37 eV. This effect is seen in the DWBA calculation and is exemplified by the Gamow factor correction which discourages electrons going close to each other and thus suppresses the binary peak relative to the recoil.

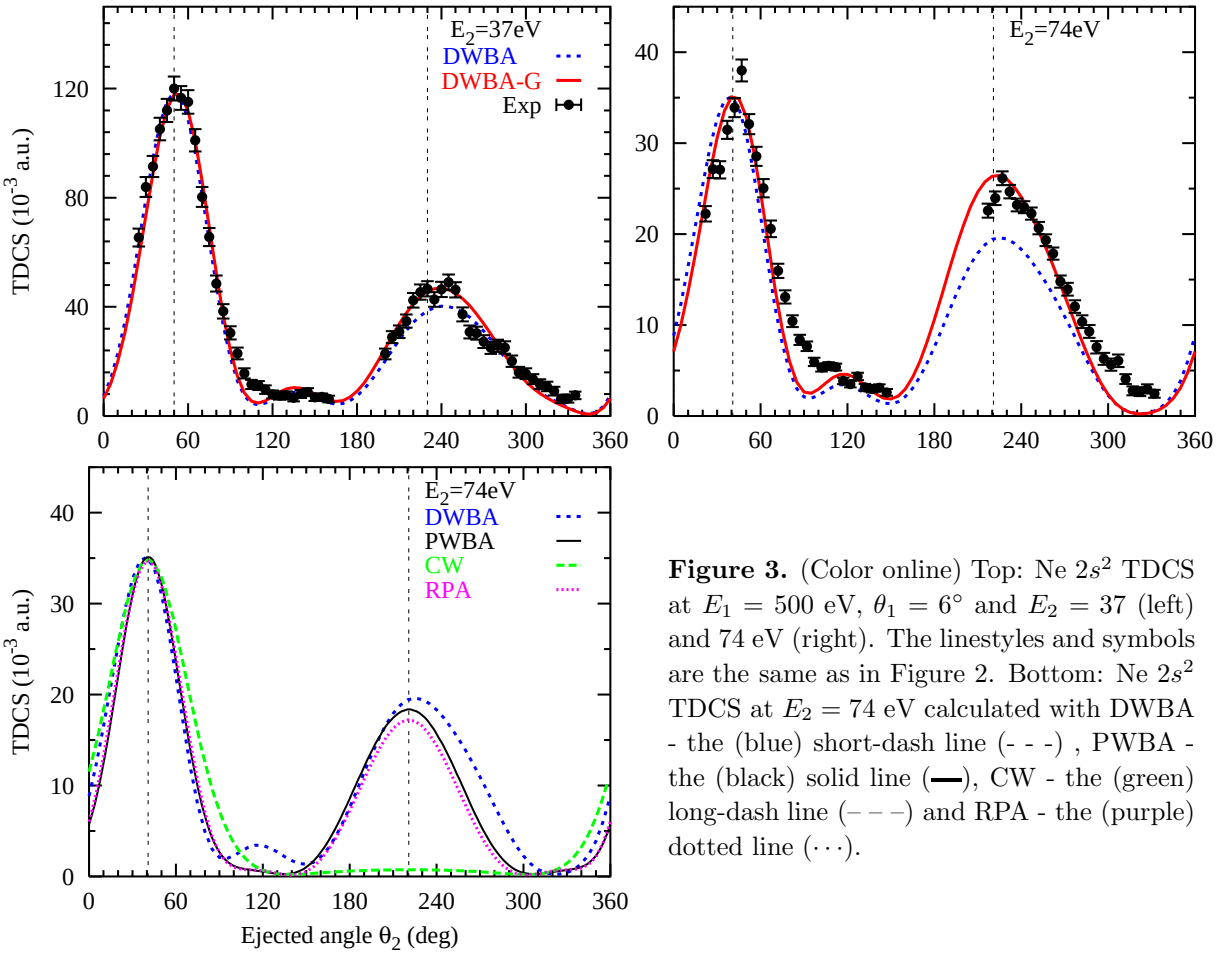

Figure 3. (Color online) Top: Ne $2s^2$ TDCS at $E_1 = 500$ eV, $\theta_1 = 6°$ and $E_2 = 37$ (left) and 74 eV (right). The linestyles and symbols are the same as in Figure 2. Bottom: Ne $2s^2$ TDCS at $E_2 = 74$ eV calculated with DWBA - the (blue) short-dash line (- - -) , PWBA - the (black) solid line (—), CW - the (green) long-dash line (– – –) and RPA - the (purple) dotted line (· · ·).

To investigate this effect further, on the bottom panel of Figure 3, we present yet three other calculations of the TDCS for $E_2 = 74$ eV. One is the PWBA in which the distorting effect of the target on the projectile as well as the exchange of the scattered and ejected electrons are neglected. The PWBA calculation is normalized to the DWBA by an additional scaling factor of 0.9. We see that the PWBA calculation gives almost an identical binary-to-recoil ratio, as does the DWBA. The only significant difference from DWBA is the absence of an additional peak centered at about $\simeq 120°$. Also, both the binary and the recoil peaks are strictly symmetric with respect to the $\pm\hat{\boldsymbol{q}}$ directions as expected in PWBA.

We see that, indeed, the binary-to-recoil ratio is determined by the slow ejected electron movement in the ionic potential which is a superposition of the Coulomb potential of the nucleus and the HF potential of the ionized electron core. To discern the roles of these two components of the atomic potential, we perform yet another PWBA calculation with Coulomb waves (CW). In this calculation, the ejected electron is represented by the Coulomb waves calculated with the screened nucleus charge $Z = 1$. The CW is again normalized to DWBA. We see that the recoil peak suffered a significant loss in the CW calculation. This is so because the smooth long-range Coulomb potential alone is a poor reflector and it is the short-range HF potential that is chiefly responsible for the formation of the recoil peak. That is why the BBK-type calculations are very poor when predicting the recoil peak intensity.

The RPA calculation in which the Born matrix element (13) is modified by the inter-shell correlation between the $2s^2$ and $2p^6$ shells, is indicated in Figure 3 by a purple dotted line. The RPA result is normalized to DWBA by scaling up by a factor of 1.3. We see that the shape of TDCS in RPA is not very different from PWBA or DWBA.

Now we turn to the question why the recoil peak intensity is increasing with the ejected electron energy in the case of Ne $2s^2$ ionization. We follow the partial wave analysis given by Vriens (1969) and present the Born matrix element (14) as the sum

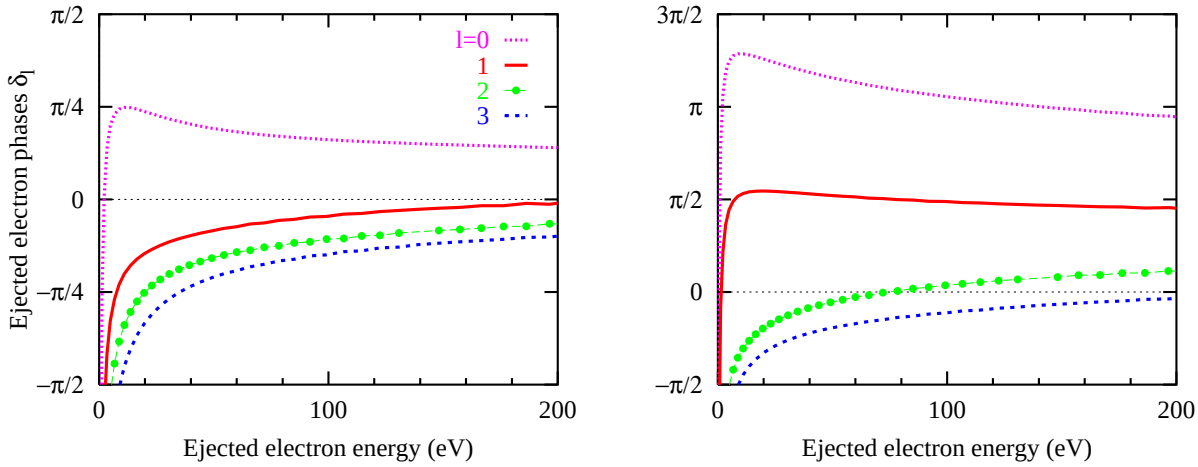

Figure 4. Ejected electron scattering phases δ_l in Equation (14) as functions of energy for He^+ (left) and Ne^+ (right). The linestyles are as follows: s-phase - the (purple) dotted line, p-phase - the (red) solid line, d-phase - the (green) filled circles and f-phase - the (blue) dashed line

of the Legendre polynomials which can be written as

$$\langle \boldsymbol{k}_2|M(\boldsymbol{q})|i\rangle = \sum_{l=0}^{3} a_l \; P_l(\cos\theta_2) \tag{16}$$
$$= (a_0 - \frac{1}{2}a_2) + (a_1 - \frac{3}{2}a_3)\cos\theta_2 + \frac{3}{2}a_2\cos^2\theta_2 + \frac{5}{2}a_3\cos^3\theta_2 \; .$$

For the s-shell ionization ($l_i = 0$) $a_l \propto e^{i\delta_l}\hat{l}^2 \int dr \, P_{El}\, j_l(qr)\, P_{ns}$. We truncate the partial wave expansion (14) at $l_{\max} = 3$ which is appropriate as $l_{\max} \simeq k_2 a$ where $k_2 = 2.3$ and $a \simeq 1$ for the outer valence shell. A near zero minima around $\theta_2 = \pi/2$ (as is seen in Figure 3) can occur only when $a_0 - \frac{1}{2}a_2 \approx 0$. Under this condition, Equation (16) reduces to

$$\langle \boldsymbol{k}_2|M(\boldsymbol{q})|i\rangle = \Big[(a_1 - \frac{3}{2}a_3) + \frac{3}{2}a_2\cos\theta_2 + \frac{5}{2}a_3\cos^2\theta_2\Big]\cos\theta_2 \tag{17}$$

Comparable intensities of the binary and recoil peaks ($\cos\theta_2 = \pm 1$), as is the case for the Ne $2s^2$ ionization, require that $|a_1 + \frac{3}{2}a_2 + a_3| \approx |a_1 - \frac{3}{2}a_2 + a_3|$ and either a_2 is very small (which implies that a_0 is very small) or is shifted in phase with respect to $a_1 + a_3$ by a factor $\pi/2$.

In Figure 4 we plot the ejected electron scattering phases δ_l, $l = 0 \ldots 3$ which determines the phases of the coefficients a_l since the radial integral in their definition is real. We notice a manifest difference between the scattering phases for He^+ (left panel) and Ne^+ (right panel). In the case of He^+, the phases δ_l, $l = 1 \ldots 3$ are close

together whereas the s-phase δ_0 is far apart. This can be explained by the presence of the occupied $1s$ state in the ionic core. For neutral atomic targets, the scattering phase at zero energy is related to the number of the occupied target states N_l by the Levinson's theorem $\delta_l(k \to 0) = N_l\pi$. For ionized targets, because of the long-range Coulomb potential tail, the Levinson's theorem does not hold. However, the phase shift due to the short range potential, i.e. the difference of the total phase and the Coulomb phase, is related to the quantum defect $\delta_l(k \to 0) - \sigma_l(k \to 0) = \mu_l(\infty)\pi$. The latter is determined by fitting the sequence of energy levels with a given orbital momentum $E_{nl} = 0.5Z_{\rm eff}[n - \mu_l(n)]^{-2}$ (Seaton 1983). Here the effective charge of the screened nucleus $Z_{\rm eff} \simeq 1$. The Coulomb phase is given by the expression

$$\sigma_l(k) = \arg\Gamma\left(1 + l - i\frac{Z_{\rm eff}}{k}\right) \quad , \quad \sigma_{l+1}(k) = \sigma_l(k) - \arctan\left[\frac{Z_{\rm eff}}{k(l+1)}\right] . \qquad (18)$$

The presence of the bound target state with a given l perturbs the energy level sequence and results in a large quantum defect. This is the case of the s-phase in He^+. The other l-phases are quite close and tend to converge at larger energies as prescribed by Equation (18). Because of this phase behaviour, the coefficients a_1, a_2 and a_3 are more or less collinear and the recoil intensity is fairly small relative to the binary peak.

The situation in Ne^+ is very different because of the bound $2p$ state which results in a large quantum defect and the p-phase deviating strongly from the d- and f-phases. We see from the right panel of Figure 4 that the phase difference between the p- and d-phases reaches $\pi/2$ at an energy of about 100 eV which is a prerequisite of the orthogonality of $a_1 + a_3$ and a_2 (a_3 is relatively small). Thus we have a large recoil-to-binary intensity ratio which increases with energy from 37 eV to 74 eV in anticipation of the maximum slightly above 100 eV.

In Figure 5 we show the TDCS for the Ne $2p^6$ shell. The measurement has been taken at three ejected electron energies E_2 = 37, 74 and 205 eV. In all cases, we see a fairly large relative recoil peak intensity which, unlike in the Ne $2s^2$ case, decreases monotonically with increasing E_2. For a p-target state, the partial wave analysis of Vriens (1969) becomes too simplistic because of two ejected electron partial waves $l \pm 1$ are contributing to the TDCS. That is why the binary-to-recoil ratio behavior in Ne

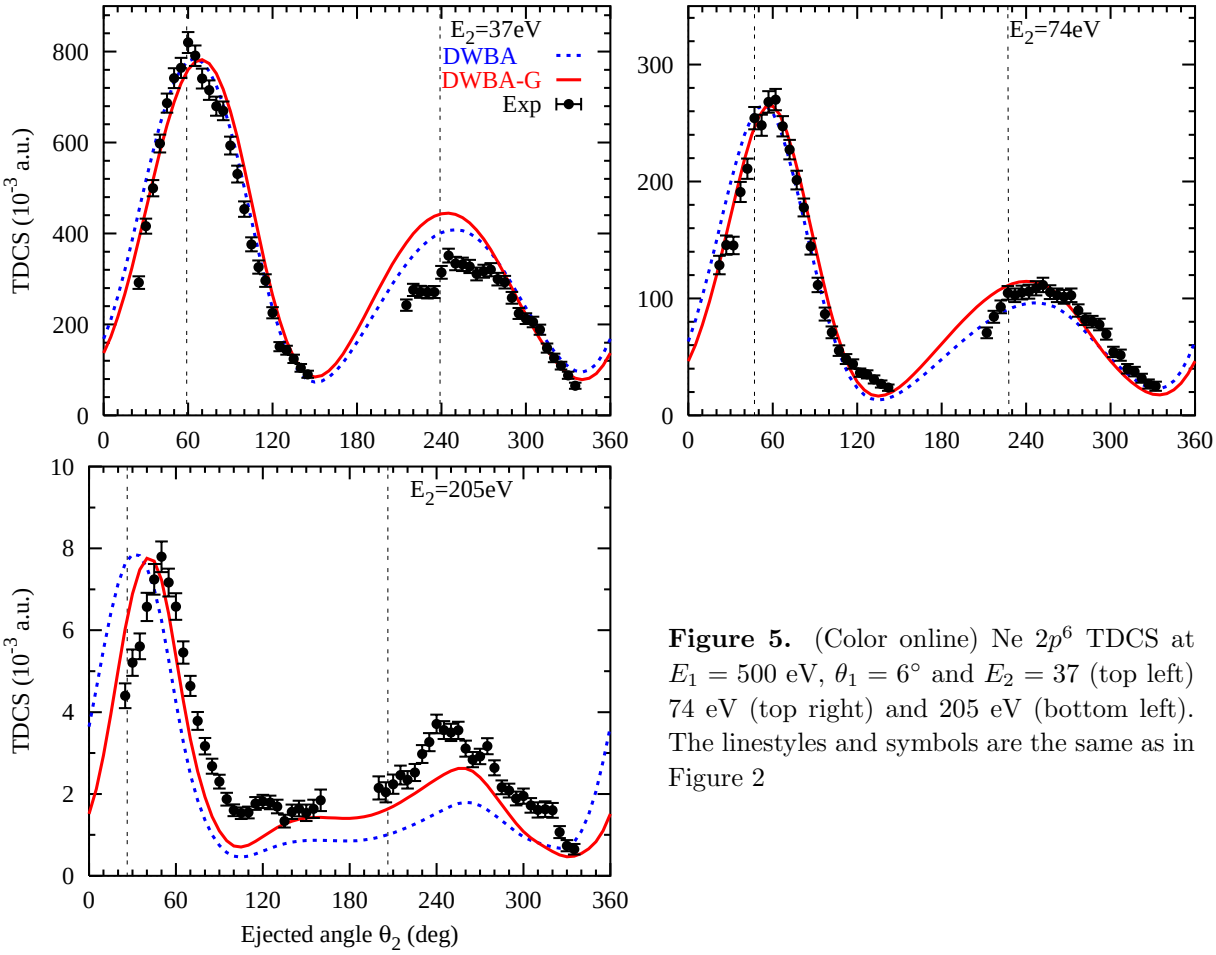

Figure 5. (Color online) Ne $2p^6$ TDCS at $E_1 = 500$ eV, $\theta_1 = 6°$ and $E_2 = 37$ (top left) 74 eV (top right) and 205 eV (bottom left). The linestyles and symbols are the same as in Figure 2

$2p^6$ is difficult to illustrate by a simple phase diagram. Nevertheless, larger recoil peak intensity in heavier noble gases beyond He can universally be attributed to the reflection from the short-range HF potential and modification of the scattering phases due to occupation of p bound states. The d-state occupation will have to be factored out in Kr and Xe which are not considered in the present manuscript.

The difference between the DWBA and renormalized DWBA-G calculations becomes progressively larger with growing E_2. It is very significant for $E_2 = 205$ eV making the calculated TDCS much closer to the experiment. The Gamow correction enhances the recoil peak intensity and shifts the binary peak away from the direction of the momentum transfer.

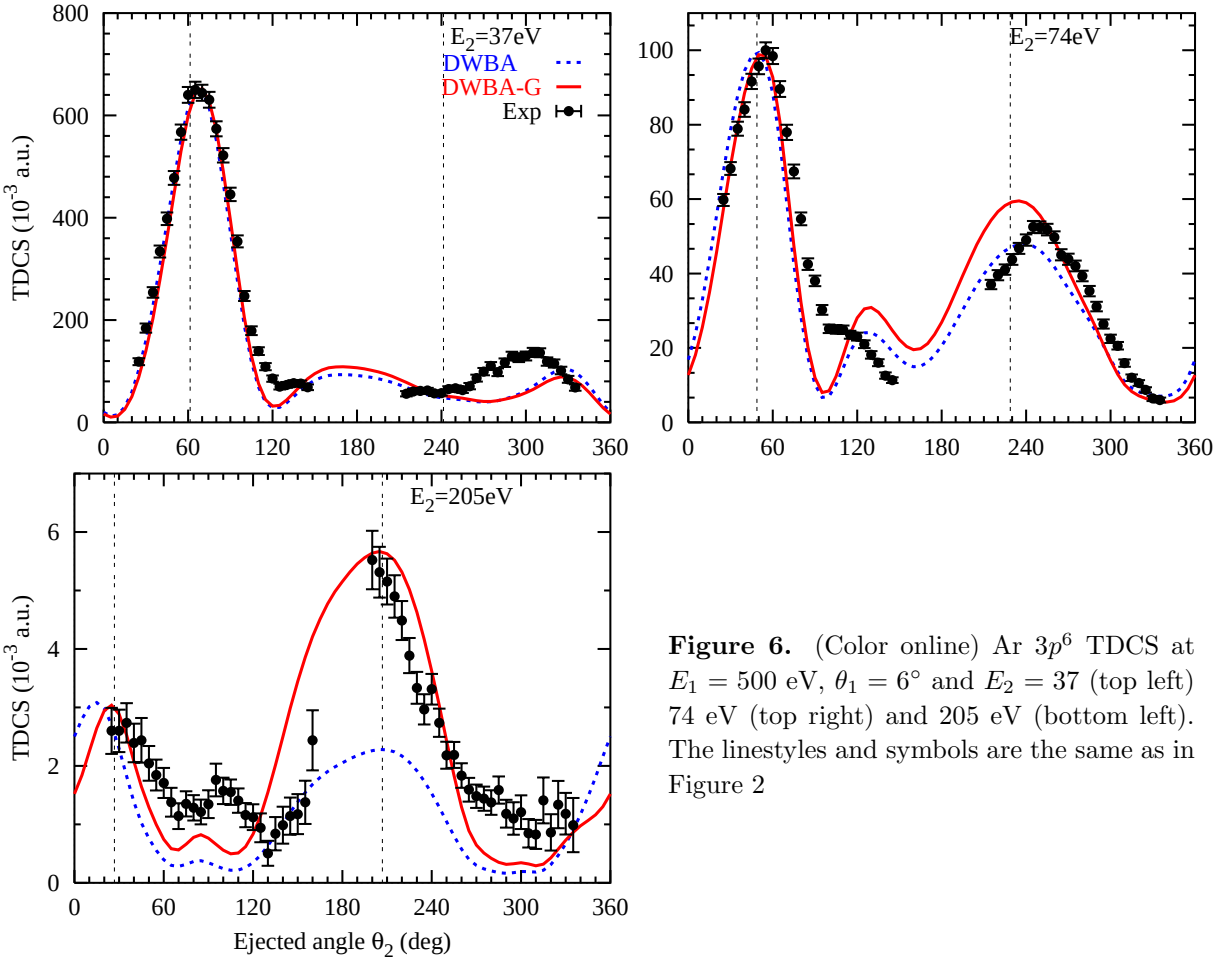

Figure 6. (Color online) Ar $3p^6$ TDCS at $E_1 = 500$ eV, $\theta_1 = 6°$ and $E_2 = 37$ (top left) 74 eV (top right) and 205 eV (bottom left). The linestyles and symbols are the same as in Figure 2

4.3. Argon

In Figure 6 we show the TDCS for the Ar $3p^6$ shell at the same ejected electron energy set of $E_2 = 37$, 74 and 205 eV and the scattered electron angle of $\theta_1 = 6°$. The experimental data for the largest energy of 205 eV have been reported previously by Catoire *et al* (2006) along with two other scattering angles of 3° and 9°. At all three values of the scattering angles, the recoil peak intensity was larger than the binary peak in manifest disagreement with the DWB-RM calculation.

As we see from Figure 6, the DWBA predicts a fairly large recoil peak intensity for $E_2 = 74$ and, especially, for 205 eV. In the latter case, the Gamow correction blows up the recoil peak which becomes significantly stronger than the binary peak, in agreement with the experiment. Although not shown in the figure, a similar agreement between the DWBA-G and experiment can be achieved for other scattering angles of 3° and 9°.

5. Conclusion

We performed a series of calculations and measurements of the fully resolved triply-differential cross-sections of the valence shells of noble gas atoms: He $1s^2$, Ne $2s^2$, $2p^6$ and Ar $3p^6$. Various theoretical models were employed which treated the projectile-target interaction to the lowest order while the account of the distorting target potential, the post-collision inter-electron interaction and the inter-shell correlation was taken non-perturbatively.

The DWBA-G model proved to be the best performer with an overall good agreement with the experiment. Some minor deviations between the calculation and measurement can still be seen. For instance, in the cases of He $1s^2$ at 205 eV, the experimental binary peak is further displaced from the $\hat{\boldsymbol{q}}$ direction and the recoil intensity is lower than theoretically predicted. Same stronger displacement is seen in the case of Ne $2s^2$ at 205 eV. Here, however, the calculation underestimates the recoil peak intensity. This means that the Gamow correction, although accounting for the bulk of the PCI, does not account for it fully. A proper non-perturbative treatment within, e.g. CCC or ECS, would probably remove this minor disagreement. We note, however, that in the case of He at 205 eV ejected energy, the CCC calculation does not account fully for the shift of the experimental binary peak from the $\hat{\boldsymbol{q}}$-direction.

Less sophisticated calculations with plane or Coulomb waves (PWBA and CW) do not produce numerically accurate results. However, when compared with DWBA, they are very indicative as to the physical mechanisms being responsible for various features of the TDCS. In particular, we analyzed the binary-to-recoil intensity ratio in terms of the partial wave phase shifts and explained an anomalously large recoil peak intensity in Ne $2s^2$ in terms of the partial waves reflection from the short-range HF potential.

The inter-shell correlation was taken into account using the RPA model which proved to be a very effective tool in photoionization of valence shells of noble gas atoms. For the given kinematics, the effect of the inter-shell correlation was found to be insignificant. It is expected that this effect could grow for lower ejected electron energies near the ionization threshold. Also, it could be seen more clearly when normalized

experimental TDCS become available.

The present model, although successful at fairly large incident energy in excess of 500 eV, is not expected to cover the whole range of (e,2e) kinematics. Inevitably, it will break down for low incident energies when the Coulomb interaction between the projectile and the target and between the two outgoing electrons become strong. This was demonstrated in a recent DW-PCI calculation of (e,2e) on Kr $4s^2$ where E_0 was lowered from 197 eV to $E_0 = 35$ eV to witness a gradual deterioration of the accuracy of theoretical results (Haynes *et al* 2003). It is the full Coulomb inter-electron interaction, not just its asymptotic part as in the BBK formalism, that should be treated non-perturbatively to achieve numerically accurate results for the electron energies below few ionization potentials.

Acknowledgment

The authors wish to thank Prof. V K Ivanov for placing a Fortran version of the computer code by Chernysheva *et al* (1975) in their disposal. A Naja acknowledges a doctoral grant from the *Agence Universitaire de la Francophonie* (AUF).

References

Abramowitz M & Stegun I A 1975 *Handbook of mathematical functions with formulas, graphs, and mathematical tables* Academic Press New York

Amusia M Y 1990 *Atomic photoeffect* Plenum Press New York

Bartschat K & Burke P G 1987 The R-matrix method for electron impact ionisation *J. Phys. B* **20**(13), 3191–3200

Bolognesi P, Bohachov H, Borovik V, Veronesi S, Flammini R, Fainelli E, Borovik A, Martinez J, Whelan C T, Walters H R J, Kheifets A & Avaldi L 2008 The ionization of Mg by electron impact at 1000 ev studied by (e, 2e) experiments *J. Phys. B* **41**(1), 015201

Brauner B, Briggs J S, Klar H, Broad J T, Rösel T, Jung K & Ehrhardt H 1991 Triply differential cross sections for ionization of hydrogen atoms by electrons: the intermediate and threshold energy regions *J. Phys. B* **24**(3), 657–673

Bray I, Fursa D V, Kheifets A S & Stelbovics A T 2002 Electrons and photons colliding with atoms: development and application of the convergent close-coupling method *J. Phys. B* **35**(15), R117–R146

Catoire F, Staicu Casagrande E M, Lahmam-Bennani A, Duguet A, Naja A, Ren X G, Lohmann B & Avaldi L 2007 New developments for an electron impact (e,2e)/(e,3e) spectrometer with multiangle collection and multicoincidence detection *Rev. Sci. Instrum.* **78**(1), 013108

Catoire F, Staicu Casagrande E M, Nekkab M, Dal Cappello C, Bartschat K & Lahmam-Bennani A 2006 Investigation of the (e, 2e) single ionization of He and Ar at large energy loss close to minimum momentum transfer *J. Phys. B* **39**(12), 2827–2838

Chernysheva L V, Amusya M Y & Sheftel S I 1975 Program of calculating the atomic generalized oscillator strength with interelectron correlations within two transitions In Russian Report No. 495 A. F. Ioffe Institute St. Petersburg

Chernysheva L V, Cherepkov N A & Radojevic V 1976 SCFHF program *Comp. Phys. Comm.* **11**, 57

Chernysheva L V, Cherepkov N A & Radojevic V 1979 Frozen core hartree-fock programm for atomic discrete and continuous states *Comp. Phys. Comm.* **18**, 87–100

Dupre C, Lahmam-Bennani A & Duguet A 1991 About some experimental aspects of double and triple coincidence techniques to study electron impact double ionizing processes *Meas. Sci. Technol.* **2**(4), 327–333

Haynes M A, Lohmann B, Prideaux A & Madison D H 2003 Coplanar symmetric (e, 2e) cross sections for krypton 4s ionization *J. Phys. B* **36**(5), 811–815

Jones S & Madison D H 1994 Asymptotically-correct distorted-wave calculations for low-energy electron-impact ionization of helium *J. Phys. B* **27**(7), 1423–1428

Kheifets A S 1993 Triple differential cross section calculation for the helium autoionization by electron impact *J. Phys. B* **26**(13), 2053–2068

Lahmam-Bennani A 2002 Thirty years of experimental electron-electron (e,2e) coincidence studies: achievements and perspectives *J. Electron Spectrosc. Relat. Phenom.* **123**(2-3), 365–376

Landau L D & Lifshitz E M 1985 *Quantum Mechanics (Non-relativistic theory)* Vol. 3 of *Course of theoretical physics* 3rd edn Pergamon press Oxford

Madison D H, Calhoun R V & Shelton W N 1977 Triple-differential cross sections for electron-impact ionization of helium *Phys. Rev. A* **16**(2), 552–562

Mazevet S, McCarthy I E, Madison D & Weigold E 1998 Semirelativistic DWBA for the ionization of closed shell atoms at intermediate energies *J. Phys. B* **31**(10), 2187–2202

McCarthy I E 1995 Distorted-wave Born and impulse approximations for electron-atom ionization *Aust. J. Phys.* **48**(1), 1–17

McCarthy I & Weigold E 2005 *Electron-Atom Collisions* Cambridge University Press Cambridge

Naja A, Staicu Casagrande E M, Lahmam-Bennani A, Nekkab M, Mezdari F, Joulakian B, Chuluunbaatar O & Madison D H 2007 Triply differential (e,2e) cross sections for ionization of the nitrogen molecule at large energy transfer *J. Phys. B* **40**(18), 3775–3783

Naja A, Staicu Casagrande E M, Lahmam-Bennani A, Stevenson M, Lohmann B, Dal Cappello C, Bartschat K, Kheifets A, Bray I & Fursa D V 2008 (e, 2e) triple differential cross-sections for ionization beyond helium: the neon case at large energy transfer *J. Phys. B* **41**(8), 085205

Nakel W & Whelan C T 1999 Relativistic (e, 2e) processes *Phys. Rep.* **315**(6), 409–471

Rescigno T N, Baertschy M, Isaacs W A & McCurdy C W 1999 Collisional breakup in a quantum system of three charged particles *Science* **286**, 2474–2479

Rouvellou B, Rioual S, Röder J, Pochat A, Rasch J, Whelan C T, Walters H R J & Allan R J 1998 Coulomb three-body effects in electron-impact ionization of argon *Phys. Rev. A* **57**(5), 3621–3626

Samardzic O, Braidwood S W, Weigold E & Brunger M J 1993 Satellite structure of the neon valence shell by electron-momentum spectroscopy *Phys. Rev. A* **48**(6), 4390–4399

Schulz M & Madison D H 2006 Studies of the few-body problem in atomic break-up processes *Int. J. Mod. Phys. A* **21**(18), 3649–3672

Seaton M J 1983 Quantum defect theory *Rep. Prog. Phys.* **46**(2), 167–257

Staicu Casagrande E M, Naja A, Mezdari F, Lahmam-Bennani A, Bolognesi P, Joulakian B, Chuluunbaatar O, Al-Hagan O, Madison D H, Fursa D V & Bray I 2008 (e,2e) ionization of helium and the hydrogen molecule: signature of two-centre interference effects *J. Phys. B* **41**(2), 025204

Varshalovich D A, Moskalev A N & Khersonskii V K 1988 *Quantum theory of angular momentum* 1st edn World Scientific Philadelphia

Vriens L 1969 Angular correlation of scattered and ejected electrons in ionizing collisions *Physica* **45**(3), 400–406

Whelan C T, Allan R J, Walters H R J & Zhang X 1993. In *(e, 2e) and Related Processes* Whelan C T, Walters H R J, Lahmam-Bennani A & Ehrhardt H, eds Vol. 414 of *Proceedings of the NATO Advanced Research Workshop* Kluwer Dordrecht p. 1